Open Research Online

The global build-up to intrinsic edge localized mode bursts seen in divertor full flux loops in JET

Journal Item

Version: Version of Record

Link(s) to article on publisher's website:
http://dx.doi.org/doi:10.1063/1.4926592

oro.open.ac.uk

S. C. Chapman, R. O. Dendy, T. N. Todd, N. W. Watkins, F. A. Calderon, J. Morris, and JET Contributors

Articles you may be interested in

Three-dimensional simulation of H-mode plasmas with localized divertor impurity injection on Alcator C-Mod using the edge transport code EMC3-EIRENEa)
Phys. Plasmas **22**, 056106 (2015); 10.1063/1.4919393

Relationship of edge localized mode burst times with divertor flux loop signal phase in JET
Phys. Plasmas **21**, 062302 (2014); 10.1063/1.4881474
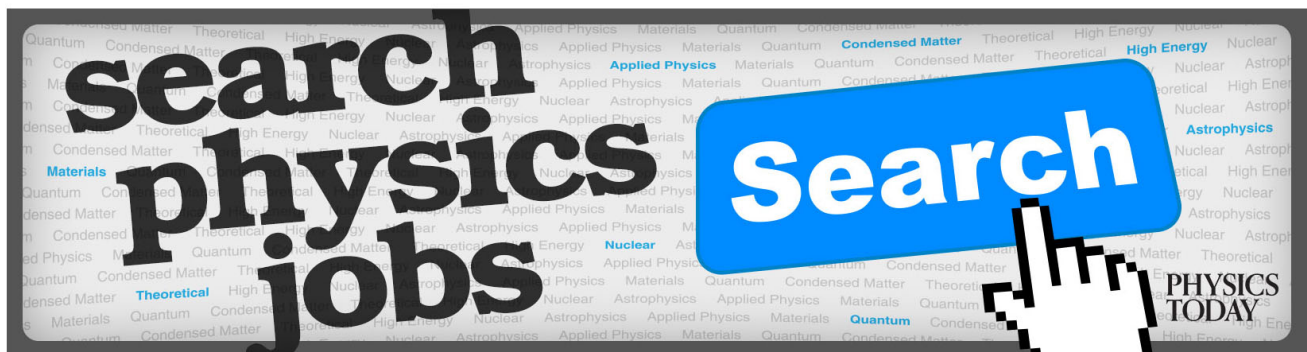
Divertor with a third-order null of the poloidal field
Phys. Plasmas **20**, 092509 (2013); 10.1063/1.4821603

The magnetic field structure of a snowflake divertor
Phys. Plasmas **15**, 092501 (2008); 10.1063/1.2967900

Transport of edge localized modes energy and particles into the scrape off layer and divertor of DIII-D
Phys. Plasmas **10**, 1765 (2003); 10.1063/1.1567723

The global build-up to intrinsic edge localized mode bursts seen in divertor full flux loops in JET

S. C. Chapman,[1,2,a)] R. O. Dendy,[1,3] T. N. Todd,[3] N. W. Watkins,[1,2,4,5] F. A. Calderon,[1] J. Morris,[3] and JET Contributors[6,b)]

[1]*Centre for Fusion, Space and Astrophysics, Department of Physics, University of Warwick, Coventry, United Kingdom*
[2]*Max Planck Institute for the Physics of Complex Systems, Dresden, Germany*
[3]*CCFE, Culham Science Centre, Abingdon, Oxfordshire OX14 3DB, United Kingdom*
[4]*Centre for the Analysis of Time Series, London School of Economics, London, United Kingdom*
[5]*Department of Engineering and Innovation, Open University, Milton Keynes, United Kingdom*
[6]*EUROfusion Consortium, JET, Culham Science Centre, Abingdon OX14 3DB, United Kingdom*

A global signature of the build-up to an intrinsic edge localized mode (ELM) is found in the temporal analytic phase of signals measured in full flux azimuthal loops in the divertor region of JET. Toroidally integrating, full flux loop signals provide a global measurement proportional to the voltage induced by changes in poloidal magnetic flux; they are electromagnetically induced by the dynamics of spatially integrated current density. We perform direct time-domain analysis of the high time-resolution full flux loop signals VLD2 and VLD3. We analyze plasmas where a steady H-mode is sustained over several seconds during which all the observed ELMs are intrinsic; there is no deliberate intent to pace the ELMing process by external means. ELM occurrence times are determined from the Be II emission at the divertor. We previously [Chapman *et al.*, Phys. Plasmas **21**, 062302 (2014); Chapman *et al.*, in *41st EPS Conference on Plasma Physics*, *Europhysics Conference Abstracts* (European Physical Society, 2014), Vol. 38F, ISBN 2-914771-90-8] found that the occurrence times of intrinsic ELMs correlate with specific temporal analytic phases of the VLD2 and VLD3 signals. Here, we investigate how the VLD2 and VLD3 temporal analytic phases vary with time in advance of the ELM occurrence time. We identify a build-up to the ELM in which the VLD2 and VLD3 signals progressively align to the temporal analytic phase at which ELMs preferentially occur, on a $\sim 2-5$ ms timescale. At the same time, the VLD2 and VLD3 signals become temporally phase synchronized with each other, consistent with the emergence of coherent global dynamics in the integrated current density. In a plasma that remains close to a global magnetic equilibrium, this can reflect bulk displacement or motion of the plasma. This build-up signature to an intrinsic ELM can be extracted from a time interval of data that does not extend beyond the ELM occurrence time, so that these full flux loop signals could assist in ELM prediction or mitigation. © 2015 Author(s). All article content, except where otherwise noted, is licensed under a Creative Commons Attribution 3.0 Unported License.
[http://dx.doi.org/10.1063/1.4926592]

I. INTRODUCTION

Enhanced confinement (H-mode) regimes in tokamak plasmas are characterized by intense, short duration relaxation events known as edge localized modes (ELMs).[1–5] Prevention of large amplitude ELMs is essential for ITER as each ELM releases particles and energy which load the plasma facing components; scaled up to ITER,[6] the largest such loads would be unacceptable. Theoretical[7,8] and observational[9] works suggest that the peeling-ballooning MHD instability of the plasma edge underlies ELM initiation, but as yet there is no comprehensive understanding of the sequence of physical processes involved in ELMing in terms of self-consistent nonlinear plasma physics.

Quantitative characterization of the dynamics of ELMing processes via their time domain properties, such as inter-ELM time intervals and ELM event waiting times, is relatively novel[10–15] and has provided evidence of unexpected structure in the sequence of ELM occurrence times. Recently,[16,17] we found that the signals from a system scale diagnostic, the toroidally integrating full flux loops in the divertor region of JET, contain statistically significant information on the occurrence times of intrinsic ELMs: the ELMs tend to preferentially occur when the full flux loop signals are at a specific analytic phase of their timeseries. Since the full flux loop signals capture aspects of the *global* plasma dynamics including large scale plasma motion, this may suggest, as first proposed in Ref. 17, a nonlinear feedback on a global scale where the control system and plasma behave as a single nonlinearly coupled system, rather than as driver and response. This feedback may act to pace the intrinsic ELMs.

---

a)Electronic mail: S.C.Chapman@warwick.ac.uk
b)See the Appendix of F. Romanelli *et al.*, Proceedings of the 25th IAEA Fusion Energy Conference 2014, Saint Petersburg, Russia.

In this paper, we investigate the time dynamics of the full flux loop signal temporal analytic phases, and directly test whether these signal phases contain information on the build-up to an intrinsic ELM. We perform direct time domain analysis of high time resolution signals from the full flux loops in the divertor region in JET. These full flux loop VLD2 and VLD3 currents are proportional to the voltage induced by changes in poloidal magnetic flux. We use a simultaneous high time resolution Be II signal to determine the intrinsic ELM occurrence times. We focus on a sequence of JET plasmas that have a steady flat top for ∼5s and which all exhibit intrinsic ELMing in that there is no deliberate intent to control the ELMing process by external means. Importantly, the full flux loop signals have sufficiently large signal dynamic range, compared to the noise, to allow the time evolving instantaneous temporal analytic phase to be determined on timescales between one ELM and the next. ELMs tend to occur preferentially at a specific temporal analytic phase in the VLD2 and VLD3 signals. Here, we find that the temporal analytic phases become progressively more strongly ordered from about 2–5 ms before the ELM up to the ELM time. Furthermore, the VLD2 and VLD3 signals become temporally phase synchronized with each other during this build-up time. Global synchronized plasma dynamics is thus part of the build-up to an intrinsic ELM. The organization of the paper is as follows: in Section II we introduce the data used in this study, in Section III we describe how the full flux loop instantaneous temporal analytic phases are determined, our main results are given in Section IV, in Section V we quantify the statistical significance of these results, and in Section VI we present a possible interpretation of these results following the scenario of Ref. 17. We provide significance tests against null hypotheses, that is, phase alignment by chance coincidence, in the Appendix.

II. ELM AND FULL FLUX LOOP TIME SIGNATURES

We analysed the sequence of JET plasmas 83769–83775 discussed in Ref. 16. These are a subset of plasmas 83630–83794 analysed in Ref. 14. Each has a flat-top H-mode duration of ∼5s. These all exhibit intrinsic ELMing in that there is no attempt to precipitate ELMs; the only externally applied time varying fields are those produced by the control system. ELM occurrence times are inferred from the Be II signal, which we will compare with measurements of the inductive voltage in the full flux loops VLD2 and VLD3. These circle the JET tokamak toroidally at a location just below and outside the divertor coils. These signals are sampled at $100\,\mu s$ time resolution, which can be compared to the shear Alfven transit time at the top of the edge pedestal which is of order a few microseconds.

The configuration of these diagnostics on JET is shown in Figure 1. The signal voltage is induced by changes in poloidal magnetic flux through the surface encompassed by the loops. We determine the ELM occurrence times t_k by identifying the peak of the Be II signal within each ELM using the method described in Ref. 16.
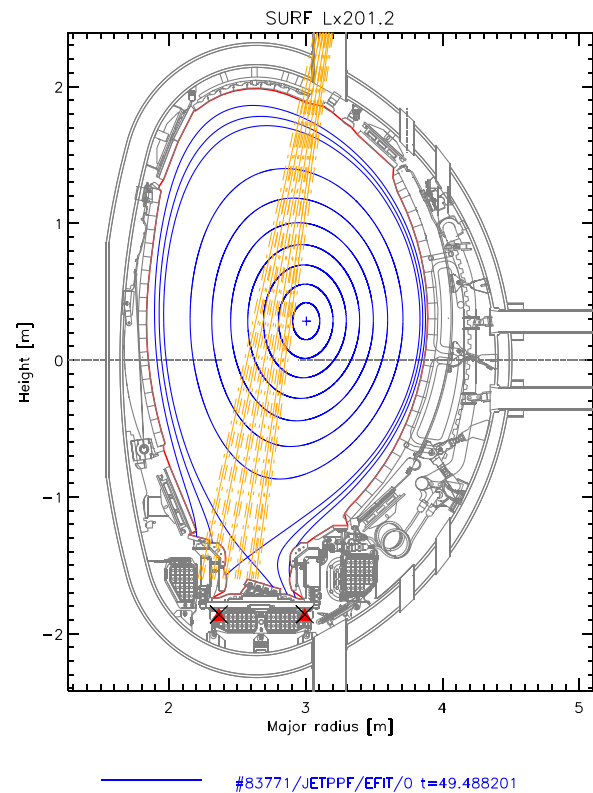

FIG. 1. Lines of sight for the BeII signal (yellow) and locations of the VLD2 and VLD3 full flux loops (red triangles) overplotted on EFIT magnetic surface reconstruction (blue lines) for JET plasma 83771 at $t = 49.49\,s$.

From the occurrence times t_k of these peaks, the time intervals between successive ELMs, the ELM waiting times, $\Delta t_k = t_k - t_{k-1}$ are found. In these plasmas, there is time structure in the probability density of ELM waiting times. There is a lower cutoff in the ELM waiting time at $\Delta t \sim 10$ms, and there are time intervals where ELMs occur less often (Ref. 16, and in other plasmas[12]). Large ensemble statistical studies across many JET plasmas have also revealed[16,17] that the ELM waiting time probability distribution shows time structure, that is, some ELM waiting times are more likely than others.

Signal traces for a representative pair of successive ELMs with a waiting time of ∼30ms are shown in Figure 2 for plasma 83771. The absolute polarity of these signals is set by convention. Following each ELM, the figures show a characteristic large amplitude oscillatory response in both of the full flux loop signals, the first cycle of which is on a timescale of ∼10ms. We previously identified[16] a class of prompt ELMs which are clustered approximately within $10 < \Delta t < 15$ms and appear to be directly paced by this response to the previous ELM. These prompt ELMs will be excluded from the current analysis, here we consider ELMs that occur on longer timescales such that this initial flux loop signal response to an ELM is seen to decay. Intervals of quasi-periodic oscillations can be seen in the VLD2 and VLD3 signals throughout the time between one ELM and the next. We will now directly obtain the instantaneous temporal analytic phase of these signals in order to test for information in these oscillations.
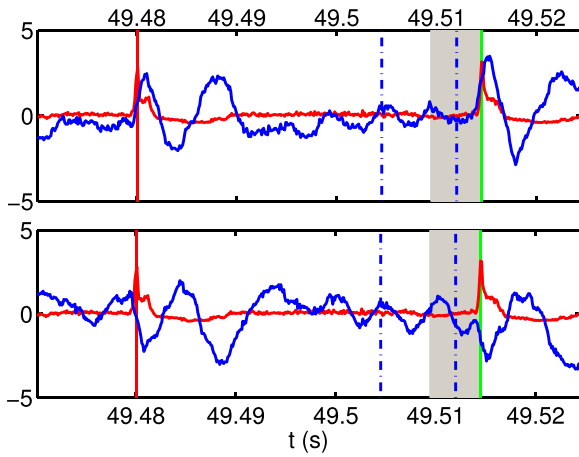
FIG. 2. Standardized traces of the raw timeseries for a pair of successive ELMs in JET plasma 83771. Time traces of Be II intensity (red) are over-plotted on full flux loops (blue) VLD3 (upper panel) and VLD2 (lower panel). To facilitate comparison, we have standardized the signal amplitudes by dividing by a multiple (10 for Be II, 2 for the VLD2 and VLD3) of their respective means over the flat-top H-mode duration, and then subtracted a local mean calculated over the interval denoted by the pair of vertical dotted-dashed blue lines. The sign convention of the VLD2 and VLD3 signals is chosen, such that they have opposite polarity. The ELM occurrence times are indicated by vertical red and green lines. For reference the time interval between 0 and 5ms before the second ELM is shaded in grey.

III. DETERMINATION OF FULL FLUX LOOP INSTANTANEOUS TEMPORAL ANALYTIC PHASE

A time series $S(t)$ has a corresponding analytic signal defined by $S(t) + iH(t) = A\exp[i\phi(t)]$, where $H(t)$ is the Hilbert transform of $S(t)$, defined in Refs. 18, 19, and 21, see also Refs. 20 and 22. This defines an instantaneous temporal analytic amplitude $A(t)$ and phase $\phi(t) = \omega(t)t$ where the instantaneous frequency is $\omega(t)$ for the real signal $S(t)$. We compute the analytic signal by Hilbert transform over each waiting time Δt_k between each pair of ELMs. The procedure is summarized in the schematic shown in Figure 3, which
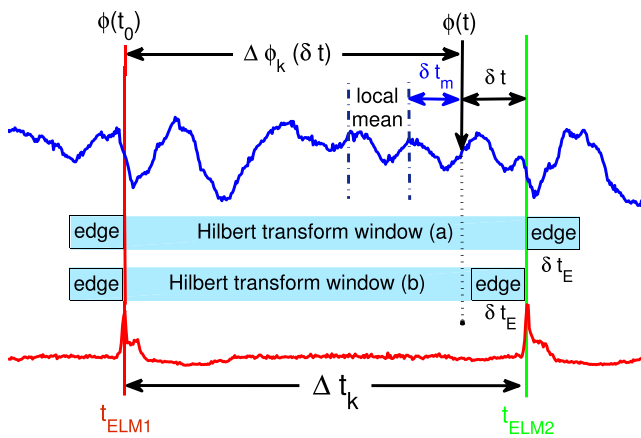

FIG. 3. Schematic (not to scale) of the procedure to determine the time dependent full flux loop difference in temporal analytic phase $\Delta\phi_k(\delta t)$ as a function of the time interval δt measured back from the time t_{ELM2} of the second ELM in an ELM pair. $\Delta\phi_k(\delta t)$ is with respect to the temporal analytic phase at the time t_{ELM1} of the first ELM. The temporal analytic phase can only be determined at times that are within the Hilbert transform window edge δt_E. One can then choose a Hilbert transform window (a) that goes beyond t_{ELM2}, so that $\delta t > 0$ or (b) that stops at t_{ELM2}, so that $\delta t > \delta t_E$.

shows the domain over which the Hilbert transform is calculated relative to a pair of ELMs occurring at $t_{k-1} = t_{ELM1}$ and $t_k = t_{ELM2}$. We will obtain the temporal analytic phase for the full flux loop signals for a sequence of times δt preceding the second ELM of each pair, that is, at times $t_{ELM2} - \delta t$. We will need to choose a zero time t_0 to define a temporal analytic phase difference in the full flux loop signals $\Delta\phi = \phi(t) - \phi(t_0)$; here t_0 will be an estimate of the occurrence time of the first ELM.

The full flux loop signals are sufficiently above the noise that we can use this method to determine their instantaneous temporal analytic phase. The instantaneous temporal analytic phase cannot be directly extracted for the Be II signal because its noise level is usually too high. We first perform a 3 point spline smoothing on the VLD2 and VLD3 time series to remove noise fluctuations on the sampling timescale. The signal analyzed must oscillate about zero in order for the instantaneous temporal analytic phase to be well determined from the analytic signal, we can ensure this locally by subtracting a locally determined mean specified as shown in Figure 2. The signal local mean is determined within a window that is shifted back in time by δt, in the results shown here we used a window $T_A = [t_k - 0.01, t_k - 0.0025]s - \delta t$, relative to each ELM occurrence time t_k (so that on the schematic $\delta t_m = 2.5$ms). The Hilbert transform has a single-sided Fourier transform which is approximated via fast Fourier transform over the finite time window of the data. We therefore need to use a time window that is larger than that of the time domain of interest to avoid edge effects, so that we only calculate the instantaneous temporal analytic phase at times within a window edge time interval δt_E of the ends of the time window of data. We have found that in these time-series a $\delta t_E > 1$ms is sufficient to give stable values of the instantaneous temporal analytic phase and all results presented here use this value of δt_E. We have varied T_A, δt_m, and δt_E to check the robustness of our results.

The above methods are only effective if the full flux loop signals have good signal/noise, do not have too large a dynamic range in response to all the ELMs, and if the mean of the signal does not vary too rapidly. The high rate of change of instantaneous temporal analytic phase with time of the full flux loop signals requires well defined ELM occurrence times in order to cleanly determine any phase relationship.

IV. FULL FLUX LOOP INSTANTANEOUS TEMPORAL ANALYTIC PHASE AND BUILD-UP TO AN ELM

We will first discuss results using Hilbert transform window (a) which extends beyond the time t_{ELM2} of the second ELM, so that we can obtain the instantaneous temporal analytic phase at times up to the ELM occurrence time. In Figure 4, we plot the instantaneous temporal analytic phase of the full flux loop signal versus time for all the ELMs in JET plasma 83771. The main figure panel plots time from t_0, that is, $\Delta t = t - t_0$ versus the instantaneous temporal analytic phase difference $\Delta\phi = \phi(t) - \phi(t_0)$ of the VLD2 signal. In Figure 4, we set $t_0 = t_{ELM1}$ the time of the first ELM as determined from the Be II signal. The first (red circle) and second
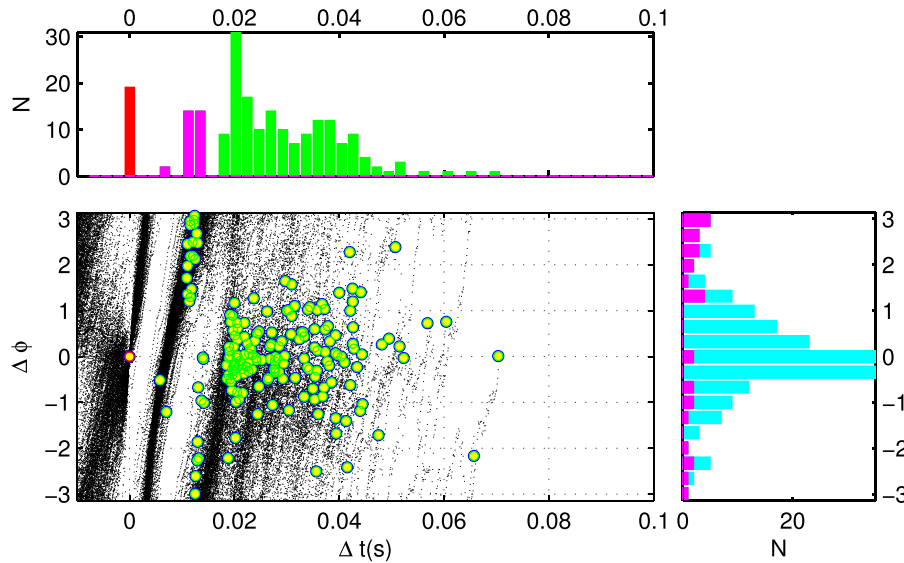
FIG. 4. ELM occurrence times and VLD2 temporal analytic phase shown for the flat-top of JET plasma 83771. The format of each set of panels is as follows: Main panel: VLD2 instantaneous temporal analytic phase, modulo 2π, plotted as a function of time following each ELM up to the occurrence time of the next ELM. The coordinates are time $\Delta t = t - t_0$ and difference in temporal analytic phase $\Delta\phi = \phi(t) - \phi(t_0)$, where $t_0 = t_{ELM1}$. ELM occurrence times are marked on each VLD2 trace with yellow-filled red circles (first ELM) and yellow-filled green circles (second ELM). Right hand panel: histogram of VLD2 $\Delta\phi$ at the time of all the second ELMs (blue), overplotted (pink) for the prompt ELMs with waiting times $\Delta t < 15$ms. Top panel: histogram of ELM occurrence times $\Delta t = t - t_0$ for the first ELM (red) and the second ELMs (green), overplotted (pink) for the prompt ELMs. The frequency N of first ELM times has been rescaled by 1/10.

(green circle) ELM times, as determined from the Be II signal, are overplotted on each corresponding VLD2 trace. On the plot, the first ELM has coordinates $\Delta t = 0$ and $\Delta\phi = 0$ by definition. The coordinates of the second ELM are the waiting time $\Delta t_k = t_{ELM2} - t_{ELM1}$ and corresponding temporal analytic phase difference $\Delta\phi_k = \phi(t_{ELM2}) - \phi(t_{ELM1})$. Histograms are shown of the waiting times Δt_k (top panel) and differences in temporal analytic phase $\Delta\phi_k$ (right panel) for all the $k = 1, ..., N$ ELM pairs. There is a group of prompt ELMs[16] with $\Delta t < 15$ms, indicated by pink bars, which are distinct in both arrival time and temporal analytic phase. We have previously identified these prompt ELM events as being directly correlated with the response to the previous ELM and will exclude them from the analysis to follow by only considering ELM pairs with waiting times $\Delta t > 15$ms. These ELMs, with $\Delta t > 15$ms, are bunched in temporal analytic phase with a peak around zero. We obtain the same results for the VLD3 and for the other plasmas in the sequence.

ELMs are thus more likely to occur when the full flux loop signals are at a specific temporal analytic phase with respect to that of the preceding ELM. Prompt ELMs occur within the coherent (in amplitude and temporal phase) response to the previous ELM which can clearly be seen in the full flux loop signals.[16] For all other, non-prompt ELMs, the full flux loop signals do not remain coherent in both amplitude and temporal phase throughout the inter-ELM time interval. The question is then whether there is detectable temporal phase coherence at all times (implying that the system retains a memory of the preceding ELM) or whether temporal phase coherence is lost, and then re-emerges as part of the build-up to the next ELM. Figure 5 shows polar plots of the histogram of the temporal analytic phase differences $\Delta\phi_k(\delta t)$ for all of the ELM pairs in plasma 83771. The temporal analytic phase difference is determined at time

$t = t_{ELM2} - \delta t$, that is, at time δt before the second ELM. As the preceding ELM generates a large amplitude response in the full flux loop signals on a timescale ~ 10ms, we will exclude ELM pairs with waiting times $\Delta t < 15$ms $+ \delta t$; hence the number N of samples in the histogram decreases with increasing δt. As in Figure 4, we use Hilbert transform window (a) which extends beyond the time t_{ELM2} of the second ELM, so that we can obtain the instantaneous temporal analytic phase at times up to the ELM occurrence time. The bottom panels in Figure 5 are at the time of the ELM, $\delta t = 0$, so that the bottom left hand plot is a polar histogram of the same data as in the right hand panel of Figure 4. The time before the ELM δt increases moving up the plot. We then see that the temporal analytic phase difference qualitatively becomes progressively more ordered from $\delta t \sim 5$ms and that there is a clear temporal phase bunching after $\delta t \sim 2$ms. This suggests that there is a signature of the build-up to an ELM in the full flux loop signals and we will quantify the degree of temporal phase bunching in Sec. V.

Figures 4 and 5 required a Hilbert transform window (a) which extended beyond the time t_{ELM2} of the second ELM, so that the instantaneous temporal analytic phase at times up to the ELM occurrence time could be calculated. As a check on the robustness of the ELM build-up signature, we repeat the analysis with Hilbert transform window (b) which stops at the time t_{ELM2} of the second ELM, so that only information before the ELM occurrence time is used. The resulting polar histograms are shown in Figure 6, where apart from the different Hilbert transform window, the data and analysis are the same as that used to produce Figure 5. Now, we can only consider times before the second ELM $\delta t > \delta t_E = 1$ms. Nevertheless, we still see in these histograms a clear temporal phase bunching on the same timescales as in Figure 5, where information from times beyond the ELM time t_{ELM2} was used.
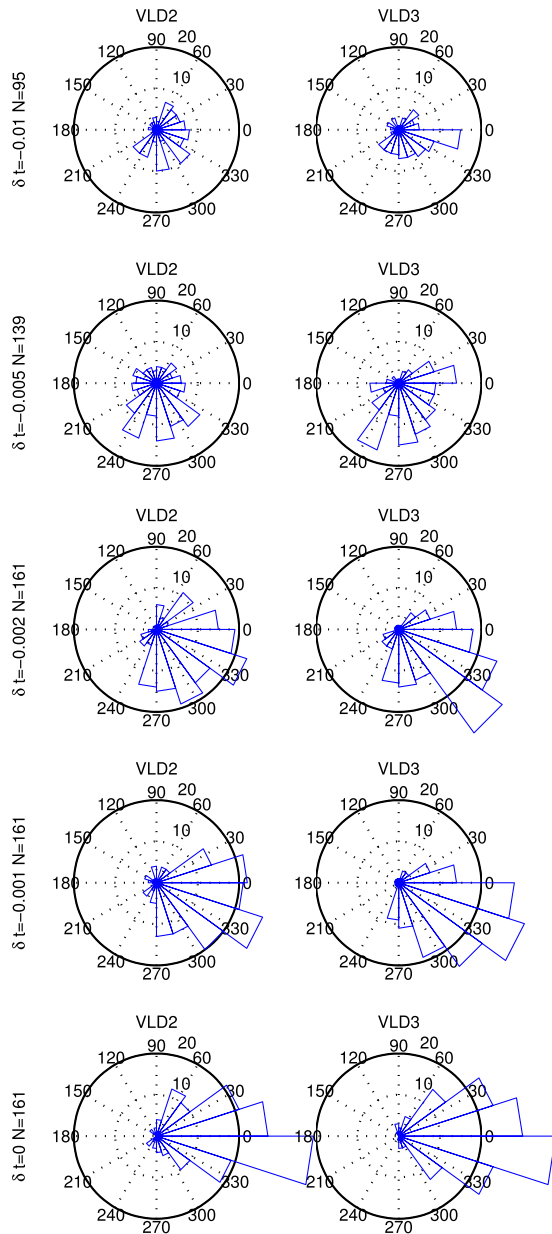
FIG. 5. Polar plots of histograms of VLD2 (left panels) and VLD3 (right panels) temporal analytic phase difference $\Delta\phi$ just before an ELM in the flat-top of JET plasma 83771. The phase difference is calculated from the time of the first ELM to a time δt before the second ELM, so that $\Delta\phi = \phi(t_{ELM2} - \delta t) - \phi(t_{ELM1})$. From bottom to top $\delta t = [0, 1, 2, 5, 10]$ms. The histograms include all ELM pairs with waiting times $\Delta t > 15\text{ms} - \delta t$, the number N in the histogram decreases with increasing δt. Hilbert transform time window (a) is used to determine the VLD temporal analytic phases and it extends $\delta t_E = 1$ms beyond t_{ELM2}, the time of the second ELM. The interval used to determine the VLD signal means just before the ELM moves back with δt.
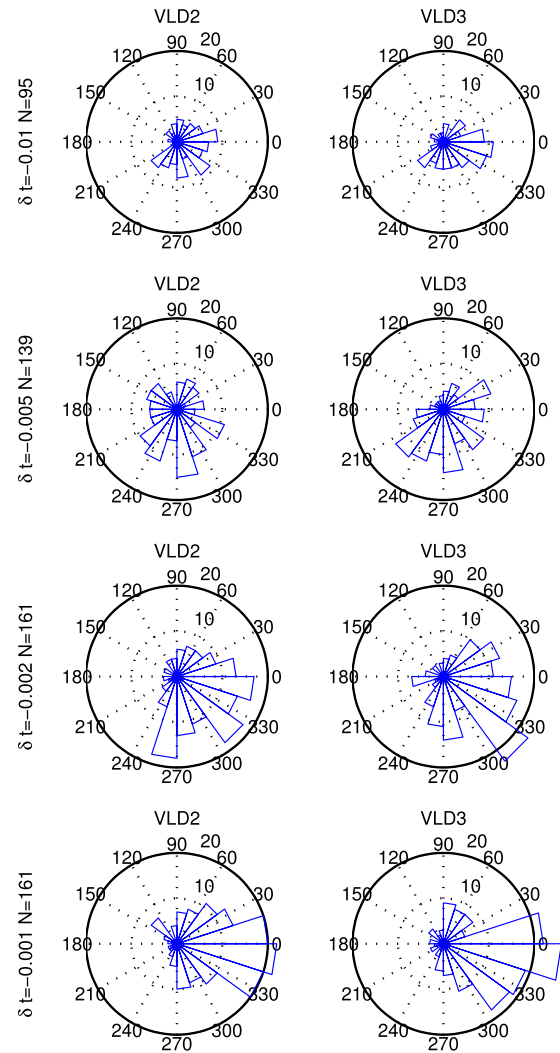

FIG. 6. Polar plots of histograms of VLD2 (left panels) and VLD3 (right panels) temporal analytic phase difference $\Delta\phi$ just before an ELM in the flat-top of JET plasma 83771. The same data and analysis are used as in Figure 5 except that now Hilbert transform time window (b) is used to determine the VLD temporal analytic phases and it stops at t_{ELM2}, the time of the second ELM. Phase differences can then only be determined for times $\delta t > \delta t_E = 1$ms before t_{ELM2}. From bottom to top $\delta t = [1, 2, 5, 10]$ms.

The above results test for temporal coherence in the build-up to an ELM, that is, over what time interval do we always see the same temporal analytic phase in the VLD2 or VLD3 just before an ELM. The VLD2 and VLD3 full flux loops are both in the divertor region of JET and in Figure 2 we can see that they are very similar in their time variation, however they are not identical. The time evolving difference in temporal analytic phase between these signals provides a measure of spatial coherence, that is, coherent large scale

plasma motion in the region of these full flux loops will tend to make their phases align. We test this idea in Figure 7 where we plot polar histograms of the instantaneous temporal analytic phase difference between the VLD2 and VLD3 signals at times δt before each of the ELMs in plasma 83771, in the same format as Figure 5. From the top panel, we see that their temporal analytic phase difference at all times shows some alignment, it is within $\sim\pm60°$ of its mean at $\delta t = 10$ms before the ELM. However, again for times $\delta t < 5$ms, that is, just before the ELM, we see that the phase difference in these two signals tends to zero, that is, they become temporally phase synchronized.

V. CIRCULAR STATISTICS AND THE RAYLEIGH TEST

We use the Rayleigh test and associated circular statistics (see, e.g., Refs. 23 and 24, and references therein) to quantify the extent to which the temporal analytic phase
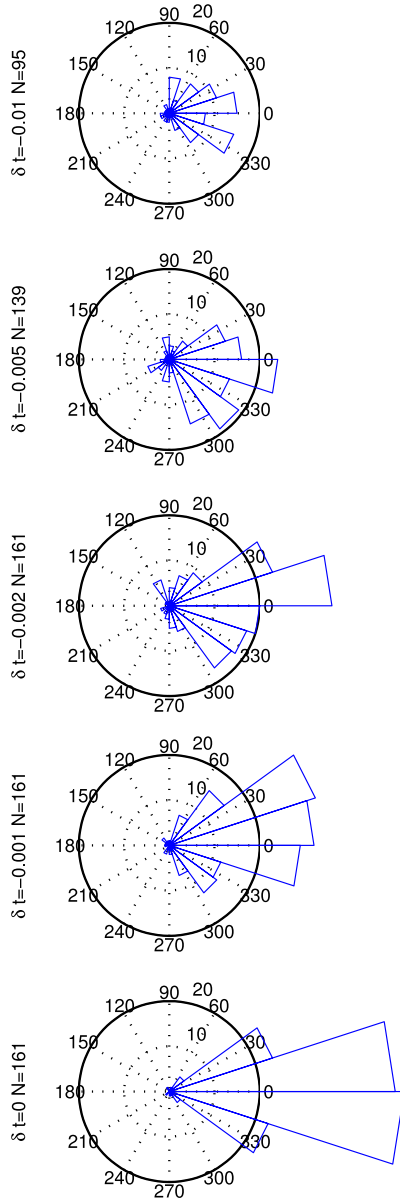
FIG. 7. Polar plots of histograms of the difference instantaneous temporal analytic phase between the VLD2 and VLD3 signals just before an ELM in the flat-top of JET plasma 83771. The temporal phase difference is calculated directly between the two signals, so that $\Delta\phi = \phi(VLD2(t)) - \phi(VLD3(t))$. The format is the same as in Figure 5. Hilbert transform window (a) is used to determine the phases.

differences are aligned, and the statistical significance of any such alignment. Using the procedure described above, we determine the temporal analytic phase differences $\Delta\phi_k$ for the $k = 1, ..., N$ ELM pairs in given plasma. If each temporal phase is represented by a unit vector $\underline{r}_k = (x_k, y_k) = (\cos\Delta\phi_k, \sin\Delta\phi_k)$, then a measure of their alignment is given by the magnitude of the vector sum, normalized to N. This is most easily realized if we use unit magnitude complex variables to represent the $\underline{r}_k = e^{i\Delta\phi_k}$. Then if

$$\sum_{k=1}^{N} \underline{r}_k = re^{i\bar{\phi}}, \tag{1}$$

the Rayleigh number is the magnitude of the sum

$$R = \frac{1}{N}\left|\sum_{k=1}^{N} \underline{r}_k\right| = \frac{r}{N} \tag{2}$$

and the mean temporal analytic phase angle is $\bar{\phi}$. Clearly, if $R = 1$ the temporal phases are completely aligned, however $R = 0$ does not distinguish random alignment from ordered anti-alignment. We will consider two other statistics here. The first is an estimate of how closely aligned the temporal phases are with the mean phase angle. We can calculate centred trigonometric moments relative to the mean phase angle $\bar{\phi}$

$$m_q = \frac{1}{N}\sum_{k=1}^{N} e^{iq(\Delta\phi_k - \bar{\phi})} = r_q e^{i\delta\phi_q}. \tag{3}$$

We will consider $q = 2$, then the temporal analytic phase angle of $m_2^{\frac{1}{2}}$, that is, $\delta\phi_2/2$ is a measure of the angular variance around the mean $\bar{\phi}$; this can take values $[0 - \pm\pi]$. We will plot this quantity as a standardized, positive definite, angular variance $\sigma_\phi = |\delta\phi_2|/2\pi$, so that σ_ϕ is in the range of $[0, 1]$.

The second is an estimate of the p-value under the null hypothesis that the vectors are uniformly distributed around the circle which is given by

$$p = \exp\left[\sqrt{1 + 4N + 4N^2(1 - R^2)} - (1 + 2N)\right], \tag{4}$$

so that a small value of p indicates significant departure from uniformity, i.e., the null hypothesis can be rejected with 95% confidence for $p < 0.05$.

We now calculate the Rayleigh R, the standardized angular variance, and p values as a function of the time before the ELM δt, corresponding to the polar histograms above. Figure 8 corresponds to the analysis of Figure 5, where we have used Hilbert time window (a) to obtain the
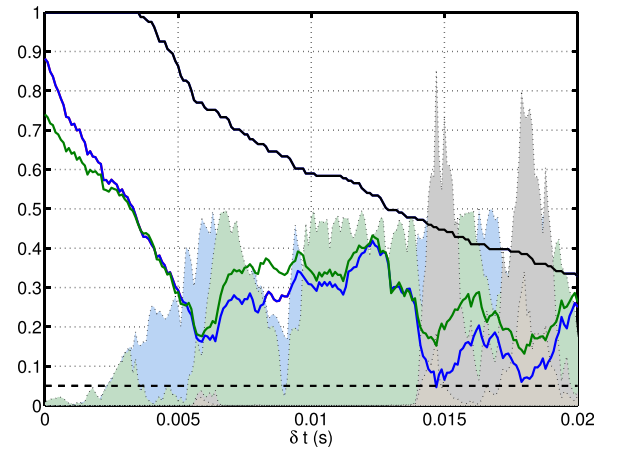

FIG. 8. Rayleigh statistics for VLD2 difference in temporal analytic phase $\Delta\phi$ just before an ELM in the flat-top of JET plasma 83771. The temporal analytic phase difference is calculated from time t_0 to a time δt before the second ELM, so that $\Delta\phi = \phi(t_{ELM2} - \delta t) - \phi(t_0)$. The figure plots variation with δt (x axis) of Rayleigh R for $t_0 = t_{ELM1}$ (green) and for $t_0 = t_{VLDmin}$ (blue). The corresponding standardized angular variance is plotted as light blue and green shading. The corresponding p-values are indicated by the dark and light grey shading, respectively. The $p = 0.05$ level is indicated by the horizontal dashed black line. The sample includes all ELM pairs with inter-ELM time intervals $\Delta t > 15ms + \delta t$, the number N in the sample decreases with increasing δt; the fraction $N(\delta t)/N(\delta t = 0)$ of ELM pairs in the sample is plotted (black). Hilbert transform window (a) is used.

VLD2 difference in temporal analytic phase $\Delta\phi_k$ at times δt just before each ELM. The temporal analytic phase difference is again calculated from the time of the first ELM to a time δt before the second ELM, so that $\Delta\phi_k = \phi(t_{ELM2} - \delta t) - \phi(t_0)$. In Figure 8, the green line is the Rayleigh R for the analysis of Figure 5 where we calculate the temporal analytic phase differences from the zero time at the first ELM $t_0 = t_{ELM1}$. The times of the extrema of the characteristic initial large amplitude oscillatory response to an ELM, which is seen in both the full flux loop signals, have been found[1] to provide a better determined zero time t_0. The blue line in Figure 8 is the R obtained for $t_0 = t_{VLDmin}$, the first minimum of the VLD2 signal following the preceding ELM. We can then see that $R > 0.3$ for $\delta t < 5$ms before the ELM occurs, and systematically increases as we approach the ELM occurrence time. Within this time interval, the standardized angular variance σ_ϕ is small, it gradually increases with δt as the temporal analytic phases become more disordered. The p-statistic remains small for times $\delta t < 15$ms indicating that the distribution of temporal analytic phases remains far from circular. However, this is not a smooth trend, there are short intervals for example, around $\delta t \sim 6$ms where $p \sim 0.05$. We have found that for $\delta t > 5$ms, the details of where short-lived fluctuations in R, σ_ϕ, and p-value occur are not robust, they vary with the dataset and with the detailed parameters of how the Hilbert transform is computed. However, the overall trends are robust, in particular, alignment of the temporal analytic phases around a single value for $\delta t < 5$ms, that is, large R and small σ_ϕ and p-value.

In Figure 6, we only used signals up to, and not beyond, the time of the ELM in order to test for the ELM build-up signature in the full flux loop temporal analytic phases. The corresponding circular statistics are plotted in Figure 9 where the temporal analytic phase differences are obtained for $t_0 = t_{VLDmin}$. The blue line in Figure 9 replots that in Figure 8, it is calculated using Hilbert transform time window (a) which extends to times beyond the ELM occurrence time. The red line in Figure 9 is obtained using the same analysis and data, but with temporal analytic phases calculated using Hilbert transform time window (b) which stops at the ELM occurrence time. We can see that the build-up to an ELM in the full flux loops can still be resolved only using information from before the ELM occurrence time.

Finally, in Figure 10 we plot the Rayleigh statistics for the difference in instantaneous temporal analytic phase between the VLD2 and VLD3 signals that was shown in Figure 7. These signals are very similar in their time variation as can be seen in Figure 2, however they are not identical. From top panel of Figure 10, we see that their temporal analytic phase difference at all times shows some alignment, it is within $\sim\pm60°$ of its mean so that $R \sim 0.5$ in Figure 10. However, again for times $\delta t < 5$ms, that is, just before the ELM, we see that the difference in temporal analytic phase between these two signals tends to zero, that is, they become temporally phase synchronized.

We have quantified the values that these circular statistics can take for these time-series due to chance coincidence. Chance coincidence can occur between time-series that have non-trivial time-structure, for example, roughly periodic
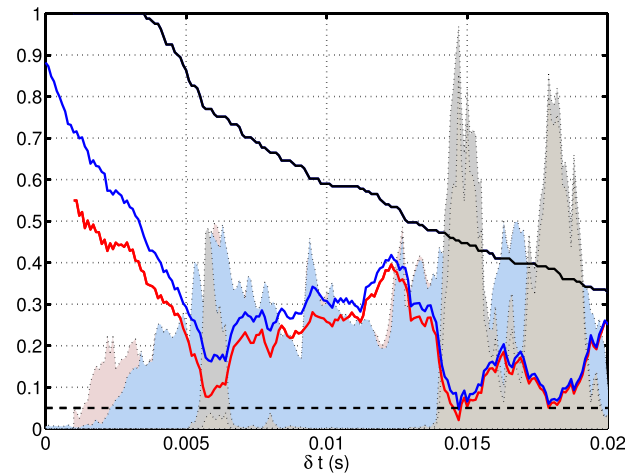

FIG. 9. Rayleigh test for VLD2 difference in temporal analytic phase $\Delta\phi$ just before an ELM in the flat-top of JET plasma 83771. The format is as in the previous figure. The temporal analytic phase difference is calculated from time t_0 to a time δt before the second ELM, so that $\Delta\phi = \phi(t_{ELM2} - \delta t) - \phi(t_0)$ where $t_0 = t_{VLDmin}$. The blue line is the same as the previous figure, Hilbert transform window (a) is used to determine the temporal analytic phases. The red line is the same analysis using Hilbert transform window (b). These time windows end at $t_{ELM2} + 1ms$ (blue) and t_{ELM2} (red), respectively. Normalized angular variance shown in shaded light blue and red, respectively. The corresponding p-values are indicated by the light and dark grey shading, respectively.

ELM occurrence times may preferentially occur at specific temporal phases of a roughly sinusoidal signal. We have constructed a set of surrogate time-series and repeated the above analysis to explore this possibility. This is described in detail in the Appendix, and establishes that the temporal phase alignments seen for times $\delta t < 5$ms can be distinguished as statistically distinct from chance occurrence and thus are evidence for correlation.

Our main result is that there is a signature of the build-up a non-prompt ELM in the temporal analytic phases of the
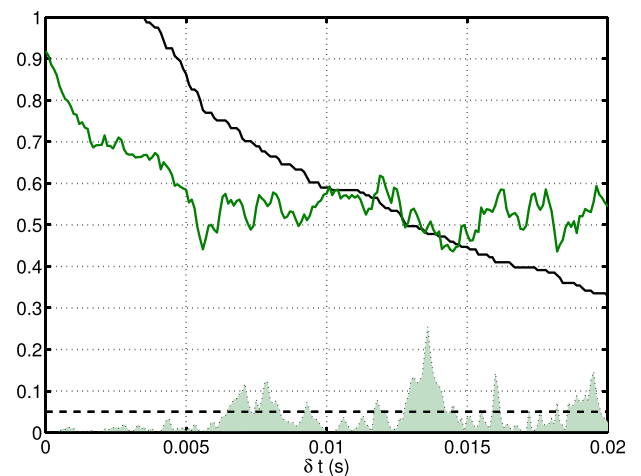

FIG. 10. Rayleigh test for the difference in instantaneous temporal analytic phase between the VLD2 and VLD3 signals just before an ELM in the flat-top of JET plasma 83771. The format is as in the previous figure. The temporal analytic phase difference is calculated directly between the two signals, so that $\Delta\phi = \phi(VLD2(t)) - \phi(VLD3(t))$. The green line is the R value, Hilbert transform window (a) is used to determine the temporal analytic phases. Normalized angular variance shown in shaded light green and the p-values by the light grey shading, here it is too small to be visible on the plot.

full flux loop signals. ELMs tend to occur preferentially at a specific temporal analytic phase in the VLD2 and VLD3 signals. The R, σ_ϕ, and p-values are all consistent with alignment of the temporal analytic phases from about 2–5 ms just before the ELM occurs. Furthermore, the VLD2 and VLD3 signals become temporally phase synchronized with each other during this build-up time. Global, spatio-temporally synchronized plasma dynamics is thus part of the build-up to an intrinsic ELM. We cannot detect statistically significant temporal phase coherence at all times, whereas we do detect temporal phase coherence re-emerging as part of the build-up to the next ELM.

VI. DISCUSSION

Our results rely upon a new approach to the analysis of an existing JET diagnostic, the full flux loops VLD2 and VLD3 signals, alongside ELM timings from the Be II signal. We have performed direct time-domain analysis of high time resolution toroidally integrating full flux loop signals arising from the dynamics of spatially integrated current density, with high time resolution determination of the ELM timings. In addition to the main results of this paper, in this section we will develop our recent conjecture[17] in the light of these results. Our aim is to frame a testable hypothesis for future work.

It is well established experimentally that ELMs can be triggered by applied magnetic "kicks" delivered by the vertical stabilization control coils which drive vertical plasma movement, including global changes in the divertor region. In such triggering experiments in JET, ELMs preferentially occur when the plasma is in a specific temporal phase in its vertical motion (downwards), and delays of ∼2–3 ms typically are observed between the start of the kick and the ELM.[25,26] Similar behaviour, i.e., ELM occurrence when the plasma is in a specific temporal phase in its vertical motion, is seen in other devices, e.g., Refs. 27 and 28, and references therein. Furthermore, the velocity perturbation associated with intrinsic ELMs is found to set a minimum threshold value that must be exceeded in order to trigger ELMs with the vertical coils.[27] The build-up to an ELM that has been magnetically kicked thus involves global plasma motion at a specific temporal phase. This global plasma displacement can then modify conditions at the plasma edge, such that peeling-ballooning and perhaps other instabilities become active, leading to the ELM burst. The details are complex and may be device dependent;[30] but the essential point here is that the kicked ELM burst follows a global perturbation in the plasma dynamics and occurs at a specific temporal phase thereof.

We have presented evidence for the emergence of coherent global dynamics in the integrated current density in the ∼2–5 ms build-up to an *intrinsic* ELM. This signature of the build up to an ELM is global, albeit perhaps poloidally localised, in that (i) it can be found in timeseries that are toroidally integrating and (ii) it is seen at both full flux loops which are at different radial positions in the divertor region. In a plasma that remains close to a global magnetic equilibrium, this can reflect bulk displacement or motion of the

plasma. We see this build-up in the full flux loop signals which track the dynamics of the integrated current density in the divertor region. The VLD2 and VLD3 signals become temporally phase synchronized during this build-up, suggesting a spatially coherent large-scale plasma perturbation. The intrinsic ELMs are found to preferentially occur at a specific temporal analytic phase in the full flux loop signals, that is, at a specific temporal phase in this global perturbation in the plasma. If this global perturbation is sufficient to modify conditions at the plasma edge to favour instability, then an intrinsic ELM can occur.

Our results suggest one possible scenario for intrinsic ELMing where the plasma and its interacting environment together self-generate a global plasma perturbation, such that the plasma is magnetically "self-kicked," which then leads to an ELM. Self-generation of global motion could occur via nonlinear feedback between the multiscale dynamics of the plasma and its interacting environment, including the control system, as we first suggested in Ref. 17. The steady state of the JET flat top plasmas is actively maintained by perturbations from the control system reacting to plasma motion. Integrated over the largest spatial scales, the reaction of the plasma to these perturbations is seen in the full flux loop signals. These signals reflect the control system and plasma behaving as a single nonlinearly coupled system, rather than as driver and response. If there were coupling between the global plasma environment, including the control system, and each of several growing modes in the plasma, these modes could become synchronized,[20–22] through their individual interactions with the global plasma/control system environment, without the need of coupling between the modes themselves. Large scale plasma motion would then develop on timescales characteristic of the dynamics of the global plasma environment. We have found an ELM build-up timescale of ∼2–5 ms, which is similar both to the ∼2ms time constant of the known unstable mode in the vertical control system on JET,[29] and the ∼2–3 ms response time to generate global plasma motion from active kicks in the vertical stabilization control coils.[25,26]

The VLD2 and VLD3 full flux loops also capture the initial integrated plasma and control system response to an ELM.[1] If this integrated plasma and control system response again corresponds to global plasma motion, it may be expected to act as a "kick" to directly trigger an ELM, if this global perturbation is sufficient to modify conditions at the plasma edge for instability. We found[16] that *prompt* ELMs sometimes occur at a specific temporal phase within this initial response to the previous ELM. This suggests an additional testable hypothesis: that compound ELMs are a pattern of successive prompt ELMs and again arise from global plasma motion emerging as above. This is consistent with the observation[12] of a narrow spread in the time intervals between successive component ELMs in a compound ELM sequence. We would then expect to see a well-defined temporal phase relationship between high time resolution full flux loop signals and the burst occurrence times within compound ELMs.

Although the above is a conjecture, it frames hypotheses that are testable by direct time-domain analysis of the

relevant signals if they can be obtained at sufficiently high time resolution, pointing to future work that may further the understanding of the ELMing process.

VII. CONCLUSIONS

We have performed direct time domain analysis of ELMing in JET plasmas where a steady H-mode is sustained over several seconds, during which there is no deliberate intent to control the ELMing process by external means. We identified the ELM occurrence times from the Be II signal and have determined their relationship with the temporal analytic phase of the VLD2 and VLD3 toroidally integrating full flux loop current signals, which are a high time resolution global measurement proportional to the voltage induced by changes in poloidal magnetic flux in the divertor region.

We have established that there is a signature of the build-up to an ELM in the temporal analytic phases of the full flux loop signals. Just before an ELM, the full flux loop temporal analytic phases progressively align such that at the ELM, they have the same value as at the previous ELM. This alignment is seen to develop over the $\sim$2–5 ms before the ELM. It is sufficiently strong that it can be distinguished from temporal phase relationships that could occur by coincidence in these quasi-oscillatory signals. We are able to recover this build-up signature using only data from before the ELM occurrence time. It thus possesses predictive power. While the full flux loops track each other at all times, that is, they have a temporal phase relationship with each other that is distinct from random, they become strongly temporally phase synchronized within this build-up time before an ELM, consistent with globally spatially coherent plasma dynamics in the divertor region.

These results may assist ELM prediction and mitigation, in that real time knowledge of the full flux loop signal temporal analytic phases indicates future times when ELM occurrence is statistically more likely. The full flux loop signals capture aspects of the global dynamics of the plasma, including large scale plasma motion, plasma dynamics in the divertor region, and mutual interaction with the control system. Our result may thus provide new insight into the ELMing process. We suggest a possible scenario that unifies our understanding of intrinsic ELMing, and magnetic pacing of ELMs that uses the vertical stabilization coils to drive bulk plasma motion.

ACKNOWLEDGMENTS

APPENDIX: SURROGATE TIME SERIES AND NULL HYPOTHESES

The full flux loop signals can be seen in the time-series to have intervals where there is a clear sinusoidal component, with a characteristic period of $\sim$10ms and the ELM waiting times have time structure; they are not random. The analysis is performed on a restricted sized sample. We now test a series of null hypotheses that capture scenarios where the temporal phase alignment that we report above could occur by coincidence. We will use the same circular statistics as above to distinguish the likelihood of coincidental occurrence in a quantitative manner. We use Hilbert transform window (a) and the same dataset as in the main paper, plasma 83771, to construct the surrogates. We have repeated this analysis for all the other JET plasmas in this sequence, and we obtain the same results.

1. ELM time and instantaneous temporal analytic phase of one full flux loop signal

We need to quantify the temporal phase alignment that could occur due to coincidence in comparing the ELM arrival times with a single signal, one of the full flux loops. If, for example, the full flux loop signals were simply monochromatic sinusoids and the ELMs occurred in a sufficiently periodic fashion, one would see ELMs preferentially occurring at particular temporal analytic phases in the full flux loop signals whether or not the sequence of ELM occurrence times and the full flux loop signals were related to each other.

We therefore test the statistical significance of the above results against some alternative hypotheses. We can represent these alternative hypotheses by constructing surrogate time-series that retain some, but not all, of the properties of the original data. We aim to test that the above results are significant compared to a random process. We also aim to quantify trivial correlation, that is, coincidences between ELM arrival time and full flux loop temporal analytic phase. Coincidences could arise in a finite dataset where both the sequence of ELM arrival times, and the full flux loop signals contain time structure that includes periodicity. Here, the ELM waiting times have a mean period and a "comb like" multi-periodic structure, and the full flux loop signals exhibit intervals of oscillatory behaviour. We will calculate the same circular statistics in exactly the same manner as above for the following surrogate datasets, the results are shown in the three panels of Figure 11.

(A) **No time correlation in the full flux loop data** (Figure 11, top panel): For each ELM pair, we randomly permute (shuffle) the order of the full flux loop time series.

(B) **No pattern in the sequence of ELM waiting times** (Figure 11, middle panel): For each ELM waiting time Δt_j, we generate a surrogate ELM waiting time Δt_s by selecting at random from the time sequence of ELM waiting times $\{\Delta t_1, \Delta t_2, ..., \Delta t_j.. \Delta t_N\}$, under the condition $\Delta t_s \leq \Delta t_j$. The surrogate set of ELM arrival times that this generates is $t_s = t_{j-1} + \Delta t_s$. Each observed ELM pair then has a corresponding surrogate temporal phase
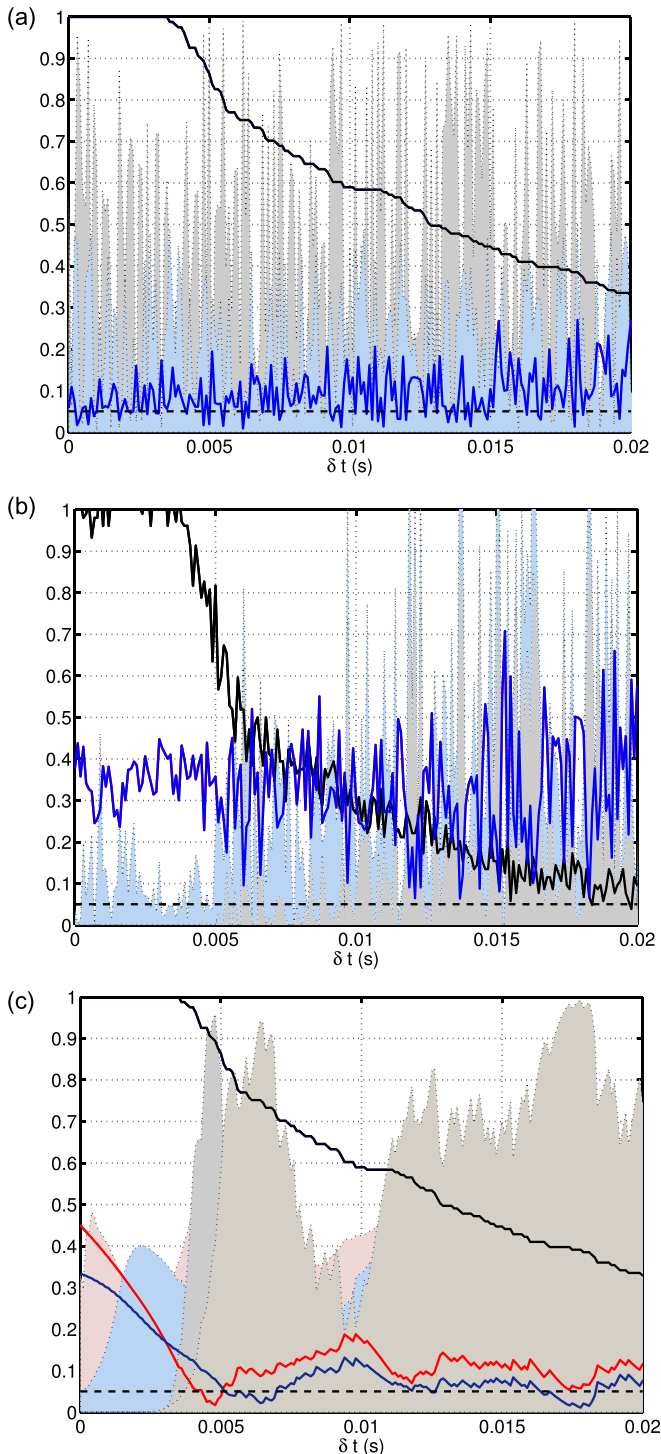
FIG. 11. Rayleigh statistics for VLD2 temporal analytic phase difference $\Delta\phi$ just before an ELM for three different surrogate time-series for the flat-top of JET plasma 83771. Format is as in previous figures. Top: the individual data points of the VLD2 signal have been randomly permuted within each ELM waiting time. Middle: the sequence of ELM waiting times is randomly permuted. Bottom: the VLD2 signal is replaced by a single sinusoid of period $T = 10$ms throughout the entire sequence of ELMs (blue); the sin temporal analytic phase is reset to zero at the time of the previous ELM (red). Red and blue shading are the normalized angular variance. Light and dark grey are the p-value of single and reset sin waves, respectively.

difference $\Delta\phi_s = \phi(t_s) - \phi(t_0)$, where t_0 is the arrival time of the first ELM and the second ELM has surrogate arrival time $t_s = t_0 + \Delta t_s$. The Δt_s is drawn from the randomly permutated set of observed ELM waiting times.

(C) **Full flux loops are single constant frequency sinusoids** (Figure 11, bottom panel): We replace the full flux loop signal with a sinusoid with period $T = 10$ms, approximately the characteristic period of the oscillatory response seen following an ELM. We trial two surrogates: the first is a single sinusoid running through the entire time-series, and second, we reset the temporal analytic phase of the sinusoid to zero at the time if the first ELM in each pair, that is, at the start of each ELM waiting time.

From these surrogates, we can conclude the following. First, surrogate A establishes the value of $R \sim 0.1$ that occurs from the temporal phases in a random signal. Here, $p > 0.05$ so that the distribution of temporal phases is indistinguishable from circular, they randomly occur at all angles. Surrogate B preserves both the full structure of the VLD2 signal and the probability distribution of ELM waiting times. Now, the ELM waiting time distribution has time structure, some waiting times occur more frequently than others. In a finite sized sample, randomly permuting them cannot generate coincidences with all possible temporal analytic phases of the VLD2 signal and this will lead to some alignment. As we move through the VLD2 time series by varying δt the degree of alignment will fluctuate. This can indeed be seen to give $R \sim 0.3$ which is larger than the random signal surrogate A. In the $\delta t \sim 5$ms before the surrogate ELM time, and both the angular variance σ_ϕ and p-value are small so that there is some alignment. This sets an upper bound for R and a lower bound for σ_ϕ which can occur by such coincidences. Finally, surrogate C produces $p > 0.05$ everywhere except $\delta t < 3$ms. For $\delta t > 3$ms, the distribution of temporal phases is indistinguishable from circular, they randomly occur at all angles. At smaller δt, there is again some alignment, which reaches a similar alignment, that is R and angular variance σ_ϕ, as in surrogate B, and for the same reason, the ELM waiting times have preferred values and these preferentially coincide with some temporal phases of the single sinusoid surrogate.

Comparing these surrogates with our result of Figure 8, we conclude that the alignment seen for $\delta t < 5$ms is statistically significant and cannot be accounted for by chance coincidence between the sequence of ELM occurrence times and the temporal analytic phase of the full flux loop signals. The alignment in $5 < \delta t < 15$ms is stronger than that of a random process ($R \sim 0.1$: surrogate A) but is comparable with that arising from temporal phase coincidence ($R \sim 0.3$, surrogates B and C) and thus cannot be distinguished from it.

2. Temporal analytic phase difference between VLD2 and VLD3 signals

The full flux loop signals both contain time structure that includes periodicity, on roughly the same period $T = 10$ms. We now test against the coincidence that could occur in the temporal analytic phase difference between sinusoidal signals sampled at a sequence of times (the ELM arrival times) that have time structure.

(A) **ELM arrives at a random time** (Figure 12, top panel): For each ELM pair, we randomly select a time within the time interval to the next ELM, that is, the second ELM arrives at a random time.

(B) **No pattern in the sequence of ELM waiting times** (Figure 12, bottom panel): We randomly permute the time sequence of ELM waiting times $\{\Delta t_1, \Delta t_2, ..., \Delta t_j .. \Delta t_N\}$ as in surrogate B above.

(C) **One of the full flux loops is a single constant frequency sinusoid** (Figure 13): We replace the VLD2 full flux loop signal with a sinusoid with period $T = 10$ms, the characteristic period of the oscillatory response seen following an ELM. We trial two surrogates, the first is a single sinusoid running through the entire time-series, and second, we reset the temporal analytic phase of the sinusoid to zero at the time if the first ELM in each pair, that is, at the start of each ELM waiting time. The results are similar, one case is shown.

FIG. 13. Rayleigh statistics for difference in temporal analytic phase between the VLD2 and VLD3 signals just before an ELM for a surrogate VLD2 time-series for the flat-top of JET plasma 83771. Format is as in previous figures. Here, we use the unchanged VLD3 and ELM arrival times. The VLD2 signal is replaced by a single sinusoid of period $T = 10$ms and the sin temporal analytic phase is reset to zero at the time of the previous ELM.

These surrogates establish that the full flux loops are similar in temporal analytic phase at all times, surrogates A and B have an $R \sim 0.5$. Comparing Figure 10, we see that this is the value at $\delta t > 5$ms.
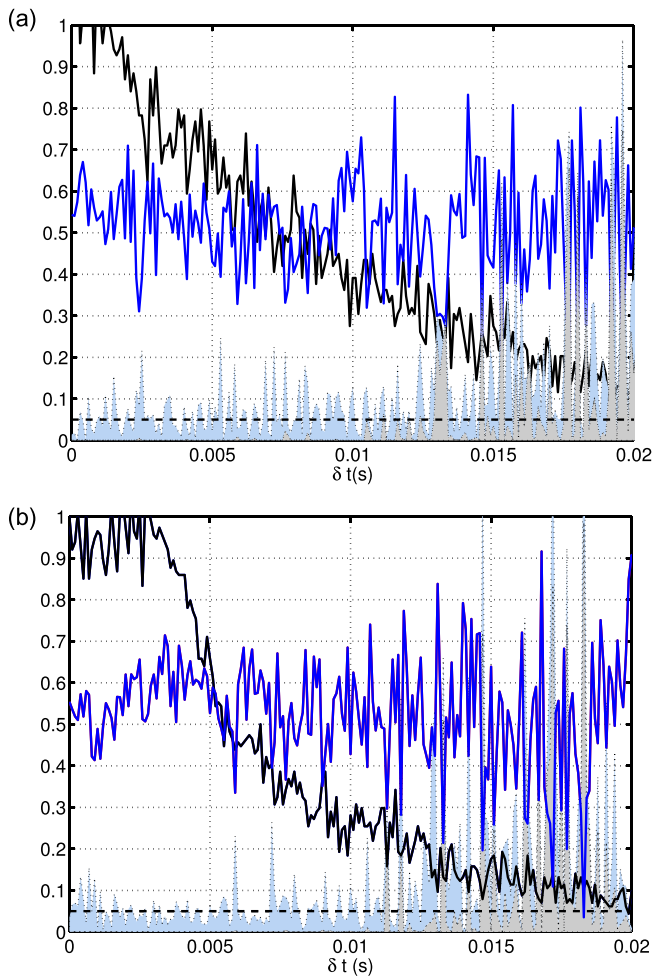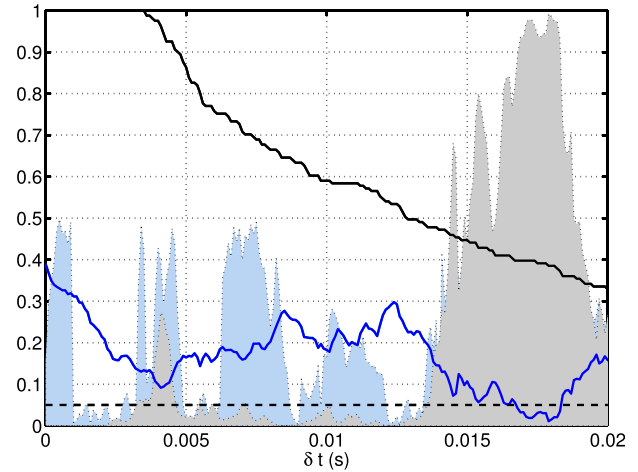

FIG. 12. Rayleigh statistics for difference in temporal analytic phase between the VLD2 and VLD3 signals just before an ELM for two different surrogate ELM time-series for the flat-top of JET plasma 83771. Format is as in previous figures. Here, we use the unchanged VLD2 and VLD3 with surrogate EM arrival times. Top: the ELM arrives randomly at any time within the observed waiting time; bottom: the ELM waiting times are randomly permuted.

[1] M. Keilhacker, Plasma Phys. Controlled Fusion **26**, 49 (1984).
[2] V. Erckmann, F. Wagner, J. Baldzuhn, R. Brakel, R. Burhenn, U. Gasparino, P. Grigull, H. J. Hartfuss, J. V. Hofmann, R. Jaenicke *et al.*, Phys. Rev. Lett. **70**, 2086 (1993).
[3] H. Zohm, Plasma Phys. Controlled Fusion **38**, 105 (1996).
[4] A. Loarte, G. Saibene, R. Sartori, D. Campbell, M. Becoulet, L. Horton, T. Eich, A. Herrmann, G. Matthews, N. Asakura, A. Chankin, A. Leonard, G. Porter, G. Federici, G. Janeschitz, M. Shimada, and M. Sugiharaet, Plasma Phys. Controlled Fusion **45**, 1549 (2003).
[5] K. Kamiya, N. Asakura, J. Boedo, T. Eich, G. Federici, M. Fenstermacher, K. Finken, A. Herrmann, J. Terry, A. Kirk, B. Koch, A. Loarte, R. Maingi, R. Maqueda, E. Nardon, N. Oyama, and R. Sartori, Plasma Phys. Controlled Fusion **49**, S43 (2007).
[6] R. J. Hawryluk, D. J. Campbell, G. Janeschitz, P. R. Thomas, R. Albanese, R. Ambrosino, C. Bachmann, L. Baylor, M. Becoulet, I. Benfatto, J. Bialek *et al.*, Nucl. Fusion **49**, 065012 (2009).
[7] J. W. Connor, Plasma Phys. Controlled Fusion **40**, 191 (1998).
[8] P. B. Snyder, H. R. Wilson, J. R. Ferron, L. L. Lao, A. W. Leonard, T. H. Osborne, A. D. Turnbull, D. Mossessian, M. Murakami, and X. Q. Xu, Phys. Plasmas **9**, 2037 (2002).
[9] G. S. Yun, W. Lee, M. J. Choi, J. Lee, H. K. Park, B. Tobias, C. W. Domier, N. C. Luhmann, Jr., A. J. H. Donn, J. H. Lee, and (KSTAR Team), Phys. Rev. Lett. **107**, 045004 (2011).
[10] A. W. Degeling, Y. R. Martin, P. E. Bak, J. B. Lister, and X. Llobet, Plasma Phys. Controlled Fusion **43**, 1671 (2001).
[11] J. Greenhough, S. C. Chapman, R. O. Dendy, and D. J. Ward, Plasma Phys. Controlled Fusion **45**, 747 (2003).
[12] F. A. Calderon, R. O. Dendy, S. C. Chapman, A. J. Webster, B. Alper, R. M. Nicol, and JET EDFA Contributors, Phys. Plasmas **20**, 042306 (2013).
[13] A. J. Webster and R. O. Dendy, Phys. Rev. Lett. **110**, 155004 (2013).
[14] A. J. Webster, R. O. Dendy, F. Calderon, S. C. Chapman, E. Delabie, D. Dodt, R. Felton, T. Todd, V. Riccardo, B. Alper, S. Brezinsek *et al.*, Plasma Phys. Controlled Fusion **56**, 075017 (2014).
[15] A. Murari, F. Pisano, J. Vega, B. Cannas, A. Fanni, S. Gonzalez, M. Gelfusa, M. Grosso, and JET EFDA Contributors, Plasma Phys. Controlled Fusion **56**, 114007 (2014).
[16] S. C. Chapman, R. O. Dendy, T. N. Todd, N. W. Watkins, A. J. Webster, F. A. Calderon *et al.*, Phys. Plasmas **21**, 062302 (2014).

[17] S. C. Chapman, R. O. Dendy, A. J. Webster, N. W. Watkins, T. N. Todd, J. Morris, and JET EFDA Contributors, in *41st EPS Conference on Plasma Physics, Europhysics Conference Abstracts* (European Physical Society, 2014), Vol. 38F, ISBN 2-914771-90-8.

[18] D. Gabor, Proc. IEE **93**(III), 429 (1946).

[19] R. N. Bracewell, *The Fourier Transform and Its Applications*, 2nd ed. (McGraw Hill, 1986).

[20] M. G. Rosenblum, A. S. Pikovsky, and J. Kurths, Phys. Rev. Lett. **76**, 1804 (1996).

[21] A. Pikovsky, M. G. Rosenblum, and J. Kurths, *Synchronization: A Universal Concept in Nonlinear Sciences* (Cambridge University Press, 2003).

[22] J. T. C. Schwabedal and A. S. Pikovsky, Phys. Rev. Lett. **110**, 204102 (2013).

[23] N. I. Fisher, *Statistical Analysis of Circular Data*, revised edition (Cambridge University Press, 1995).

[24] P. Berens, J. Stat. Software **31**, 10 (2009).

[25] E. de la Luna *et al.*, in *Proceedings of the 36th EPS Conference on Plasma Physics, Sofia, Bulgaria, 29th June–3rd July 2009*.

[26] F. Sartori *et al.*, in *35th EPS Conference on Plasma Physics, ECA, Hersonissos, 9–13 June 2008* (2008), Vol. 32D, p. 5.045.

[27] P. T. Lang *et al.*, Plasma Phys. Controlled Fusion **46**, L31–L39 (2004).

[28] S. P. Gerhardt, J.-W. Ahn, J. M. Canik, R. Maingi, R. Bell, D. Gates, R. Goldston, R. Hawryluk, B. P. Le Blanc, J. Menard, A. C. Sontag, S. Sabbagh, and K. Tritz, Nucl. Fusion **50**, 064015 (2010).

[29] Neto *et al.*, in 50th IEEE Conference on Decision and Control and European Control Conference (CDC-ECC), Orlando, FL, USA, 12–15 December 2011.

[30] S. H. Kim, M. M. Cavinato, V. Dokuka, A. A. Ivanov, R. R. Khayrutdinov, P. T. Lang, J. B. Lister, V. E. Lukash, Y. R. Martin, S. Yu Medvedev, and L. Villard, Plasma Phys. Controlled Fusion **51**, 055021 (2009).